Role of scale interactions in the abrupt change of tropical cyclone in autumn over the Western North Pacific

Pang-Chi Hsu, Ting-Hui Lee, Chih-Hua Tsou, Pao-Shin Chu, Yitian Qian & Mingyu Bi

382

🐎 Springer

Springer

CrossMark

Role of scale interactions in the abrupt change of tropical cyclone in autumn over the Western North Pacific

Pang-Chi Hsu[1] · Ting-Hui Lee[2] · Chih-Hua Tsou[3] · Pao-Shin Chu[4] · Yitian Qian[1] · Mingyu Bi[1]

Abstract Tropical cyclone (TC) activity in autumn (September–November) over the western North Pacific experienced an abrupt change in 1998, which can be detected by the Bayesian change-point analysis. During the decade before the regime shift (1988–1997), the occurrence frequency of TC genesis increased significantly over the tropical western Pacific, where the seasonal cyclonic flow, intraseasonal oscillation (ISO) and synoptic-scale eddy (SSE) were all strengthened, compared to those observed in the decade after 1998 (1998–2007). The TC trajectories also exhibited spatial differences. During the active decade, the TCs had a higher probability to move westward into the Philippine Sea and the South China Sea, and recurved northeastward toward the east of Japan. Meanwhile, the northwestward propagating TCs approaching Taiwan and southeastern coast of China were reduced. To understand the role of mean flow–ISO–SSE interaction in the decadal changes of SSE and associated TC activity, we diagnosed a newly proposed SSE kinetic energy (KE) equation that separates the contributions of seasonal-mean circulation and ISO to the SSE. The results show that, during the active TC decade, the SSE obtained higher KE from both mean flow and ISO through eddy barotropic energy conversion when the enhanced SSE momentum flux interacted with the strengthened monsoon trough and vigorous ISO cyclonic anomaly over the western tropical Pacific. The increased SSE KE contributed positively to the increased TC genesis over the main genesis region (7.5°–20°N, 130°–170°E). It also benefited the growth of TCs over the Philippine Sea and the South China Sea during the active decade. The decadal change in TC frequency over the extratropics was related to the eddy baroclinic energy conversion instead of the barotropic conversion associated with scale interaction. During the active TC decade, SSE gained more (less) KE from the SSE available potential energy over the east of Japan (the East China Sea), favoring (disfavoring) the succeeding development of TCs in this region.

1 Introduction

Tropical cyclones (TCs) severely threaten billions of people living in coastal areas. Because of such significant impacts, the long-term trend and variability of TCs have attracted tremendous attention in the recent decade (e.g., Chu 2002; Chan 2008; Maue 2011; Kossin et al. 2013; Klotzbach and Landsea 2015; Hong et al. 2016). The genesis number and destructiveness of intense hurricanes appeared to have increased due to significant warming in the Atlantic (Emanuel 2005; Webster et al. 2005). In the western North Pacific (WNP), however, the TC activity has decreased

✉ Pang-Chi Hsu
pangchi@nuist.edu.cn; pangchi.hsu@gmail.com

1 Key Laboratory of Meteorological Disaster of Ministry of Education/Joint International Research Laboratory of Climate and Environment Change/Collaborative Innovation Center on Forecast and Evaluation of Meteorological Disasters, Nanjing University of Information Science and Technology, Nanjing, China

2 National Science and Technology Center for Disaster Reduction, Taipei, Taiwan, Republic of China

3 Department of Earth Sciences, National Taiwan Normal University, Taipei, Taiwan, Republic of China

4 Department of Atmospheric Sciences, School of Ocean and Earth Science and Technology, University of Hawaii, Honolulu, HI, USA

since the mid-1990s (Liu and Chan 2013; Hsu et al. 2014; Choi et al. 2015; Lin and Chan 2015). The decrease in WNP TC activity was mostly attributed to the decadal variability in atmospheric dynamic effects, including low-level vorticity, vertical velocity and vertical wind shear, induced by sea surface temperature (SST) changes over the Indian Ocean and different regions in the Pacific basin (Hsu et al. 2014; He et al. 2015; Hong et al. 2016).

In addition to the controlling effects of large-scale atmospheric and ocean environments, the tropical synoptic-scale eddy (SSE) disturbances contribute obviously to TC formation (e.g., Chang et al. 1996; Maloney and Dickinson 2003; Chen and Huang 2009; Hsu et al. 2009; 2011; Tsou et al. 2014). Vigorous SSEs are generally related to increased TC genesis over the WNP because they may provide suitable seed disturbances for cyclogenesis (Ritchie and Holland 1999). The occurrence and amplitude of SSEs were linked to the background flow in which they are embedded (Lau and Lau 1992; Takayabu and Nitta 1993; Chen 2012). Thus, any large-scale anomalies exerted by different atmospheric variability or air-sea dynamics could modulate SSE activities and influence TC genesis. For example, the SSEs are enhanced in the southeastern section of tropical WNP during El Niño events when the warm SST and zonal wind convergence extend southeastward, resulting in increased TC genesis near the dateline (Chen and Huang 2009; Hsu et al. 2009). The intraseasonal oscillation (ISO) also plays a significant role in controlling SSE variation (Maloney and Dickinson 2003; Ko and Hsu 2009). ISO tends to transfer more energy to SSEs during the active phase than during the inactive phase (Maloney and Dickinson 2003; Ko and Hsu 2009). Thus, the amplified SSEs during the active phase of the ISO have a higher probability to intensify into TCs. In contrary, TC frequency is reduced associated with weakened SSEs during the suppressed phase of the ISO (Hsu et al. 2011; Tsou et al. 2014). These results suggest significant influences of multi-scale interaction among interannual variability, seasonal-mean flows, ISO, and SSEs on TC activities over the WNP.

Energetic analysis is an efficient and a widely used approach to quantitatively examine the interaction among different components in the atmosphere (Lau and Lau 1992; Maloney and Hartmann 2001; Maloney and Dickinson 2003; Hsu et al. 2011; Tsou et al. 2014). In earlier studies (Lau and Lau 1992; Maloney and Hartmann 2001; Maloney and Dickinson 2003), the energy conversion processes of SSEs were diagnosed by SSE kinetic energy (KE) budget equation that decomposed variables into SSEs and background mean state (including all the components with periods longer than the SSEs'). Their results explained the source of SSE KE from the background state without isolating the relative contributions of seasonal circulation and ISO to the SSEs. To distinguish the effects of mean flow

and ISO on the SSEs, some recent studies (Hsu et al. 2011; Tsou et al. 2014) further decomposed the background mean state into two components (i.e., seasonal circulation and ISO) in the SSE KE budget equation. The diagnostic results of Hsu et al. (2011) and Tsou et al. (2014) showed that SSEs could obtain KE from the seasonal-mean flows during the entire TC season. However, the ISO–SSE KE conversion varies with the phases of ISO. When the ISO is active (inactive), SSEs may gain (lose) KE from (to) the ISO through a positive (negative) barotropic energy conversion.

Most previous studies investigated SSE activity and its relation to various climate systems from a climatological perspective. At the decadal timescale, the physical mechanisms underlying how the multi-scale interactions affect the TC activity need further investigation. In this study, we attempt to diagnose the atmospheric energetic processes associated with the growth of SSEs and their contribution to autumn TC activities in the last two decades. We focus on autumn because the decadal change in TC-related features in this season is not well understood compared to those in summer over the WNP (Chang et al. 1996; Maloney and Dickinson 2003; Hsu et al. 2011; Choi et al. 2015; He et al. 2015). During a transition season like autumn, the mean flow and ISO activity may exert distinct influences on SSE and TC activity, different from the influences in summer. In addition to the contributions of scale interaction to TC genesis count, the factors affecting the distributions of TC track density at the decadal time scale will also be discussed from the perspective of atmospheric eddy energetics.

In Sect. 2, we introduce the datasets and analytical methodologies, including the three-dimensional SSE KE budget equation. In Sect. 3, we objectively detect the occurrence of regime shift for autumn TC activities. The differences in TC-related features, large-scale conditions, ISO, and SSE activities between the two decades before and after the abrupt change are then discussed. Based on the diagnostic results of SSE KE budget equation, we present in Sect. 4 how the scale interaction and heating–circulation feedback modulate the SSEs and associated TC genesis count and trajectories during the active and inactive TC decades. Finally, we summarize the contributions of atmospheric SSE energy conversion processes to the decadal change of WNP TC activity in autumn in Sect. 5.

2 Data and methodology

2.1 Datasets

To reduce the uncertainty in a TC dataset (Wu et al. 2006; Kamahori et al. 2006; Kossin et al. 2007), we collected

three best track datasets from the Regional Specialized Meteorological Center (RSMC)–Tokyo Typhoon Center of the Japan Meteorological Agency (RSMC 2013), the Joint Typhoon Warning Center (JTWC 2014) and the Shanghai Typhoon Institute (STI) of the China Meteorological Administration (CMA 2014) for studying WNP TCs. These datasets consist of TC information, such as location and intensity, at 6-h interval. Considering data quality and reliability, we only utilized the data with satellite observations from the late 1970s.

The National Centers for Environmental Prediction (NCEP)–Department of Energy (DOE) reanalysis data (Kanamitsu et al. 2002) was used to examine the influences of large-scale conditions and SSE energy processes on the decadal change in September–November (SON) TCs over the WNP. Variables used in this study include daily-averaged fields of zonal wind (u), meridional wind (v), vertical velocity (ω), temperature (T), geopotential (φ), and pressure (p) at 17 pressure levels over the period of 1979–2014. In addition, monthly-mean relative humidity and T fields were used to calculate specific humidity. These variables have a horizontal resolution of 2.5° by 2.5°. Monthly SST with a resolution of $1° \times 1°$ from the Met Office Hadley Centre (HadISST1; Rayner et al. 2003) is also used to analyze the ocean conditions. Previous studies (Suhas et al. 2012; Hsu and Yang 2015) compared atmospheric energetic features and related conversion processes in the Asian monsoon region using different reanalysis datasets. These studies showed that the results from the NCEP–DOE and ERA–interim reanalysis are highly consistent. Therefore, only the NCEP–DOE data are used in this study to examine eddy energetics.

2.2 Estimation of TC activity

In this study, all TCs with the maximum sustained wind greater than or equal to 34 knots are considered. A TC system is considered as typhoon when its sustained wind speed was greater than or equal to 64 knots. Note that the RSMC-Tokyo, JTWC and STI recorded 10-min, 1-min and 2-min sustained wind speeds, respectively. To unify the wind speed threshold for TC/typhoon detections in the three datasets, we adjusted the 10-min sustained wind in the RSMC-Tokyo to 1-min sustained wind by multiplying a ratio of 0.8 (Simiu and Scanlon 1978), similar to the approach used in the International Best Track Archive for Climate Stewardship (IBTrACS) project and operational centres (Knapp et al. 2010). Hence, the thresholds of wind speed to detect TC and typhoon cases in the RSMC-Tokyo are 30 and 56 knots, respectively. The 2-min sustained wind in the STI was converted to 1-min sustained wind based on their statistical relationship documented in Song et al. (2010).

The position at which the maximum wind speed of a TC reaches 34 knots in the JTWC is defined as the location of TC genesis. The frequency of TC occurrence is counted at each grid of $2.5° \times 2.5°$ based on the TC records at 6-h interval. The lifespan of TC is defined as the period from TC genesis to the time of TC dissipation or extratropical transition. According to Bell et al. (2000), the accumulated cyclone energy (ACE) is defined as the summation of squares of the maximum wind speed at 6-h interval.

2.3 Diagnostic energy equations

Similar to Hsu et al. (2011) and Tsou et al. (2014), we decompose an arbitrary field into three parts in the time domain, including the seasonal-mean flow (90 days), ISO (10–90 days) and SSE (<10 days):

$$A = \tilde{A} + A_I' + A_S', \qquad (1)$$

where the tilde denotes the seasonal (SON) mean component, and the prime denotes the deviation from the seasonal mean; the transient eddies include all components with a period shorter than the seasonal-mean flow (90 days), such as the 10–90-day ISO (with the subscript I) and the <10-day SSEs (with the subscript S). Here, we applied the orthonormal wavelet transform (Daubechies 1988) to extract the ISO and SSE signals from the raw data.

By multiplying u_S' and v_S' on both sides of the horizontal momentum equations, respectively, and applying a time average over a 10-day interval (denoted by an overbar), the SSE KE budget equation is obtained as

$$\frac{\overline{\partial K_S'}}{\partial t} = \underbrace{-\overline{V_S' \cdot [(V_S')_3 \cdot \nabla_3]\tilde{V}}}_{CK_{M-S}} \underbrace{-\overline{V_S' \cdot [(V_S' + V_I')_3 \cdot \nabla_3]V'}}_{CK_{I-S}}$$

$$\underbrace{-\frac{R}{P}\overline{T_S'\omega_S'}}_{CE} \underbrace{-\overline{V_3 \cdot \nabla_3 K_S'}}_{AK} \underbrace{-\overline{\nabla_3 \cdot (V_S'\varphi_S')}}_{BG} + D,$$

$$(2)$$

where $K_S' = (u_S'^2 + v_S'^2)/2$ presents the SSE KE and t is time. V indicates the horizontal wind vector. ∇ and ∇_3 indicate the two- and three-dimensional gradient operators, respectively. R is the gas constant. P is pressure. D includes the dissipation and subgrid-scale effects. According to Eq. (2), several processes can modulate the KE of SSEs. Terms CK_{M-S} and CK_{I-S} represent the barotropic energy conversion from the mean flow and ISO to SSEs, respectively. The sum of CK_{M-S} and CK_{I-S} is identical to the SSE barotropic energy conversion (CK) documented by previous studies (Lau and Lau 1992; Maloney and Dickinson 2003; Hsu et al. 2009). CE is the baroclinic energy conversion process related to the interaction between SSE temperature and vertical motion. A positive CE conversion from

SSE available potential energy to SSE KE occurs when an air parcel ascends in a warmer region or descends in a colder area. AK indicates the advection of SSE KE induced by the mean flow and transient eddies. The convergence of SSE geopotential fluxes can also induce an increased SSE KE, as shown in term BG.

Note that only terms CK (CK_{M-S} and CK_{I-S}) and CE represent the major sources of SSE KE via generation and conversion processes. Other terms are related to redistribution of SSE KE. Thus, we will focus on terms CK and CE in this study. The contributions of mean flow–SSE interaction and ISO–SSE interaction to the changes in SSE KE during different decades will be examined through comparing terms CK_{M-S} and CK_{I-S}.

2.4 Statistical analysis methods

The Bayesian paradigm under the one change-point hypothesis is used to identify the timing of an abrupt change in autumn TC activity (Chu and Zhao 2004; Hsu et al. 2014). The distribution of the seasonal count of typhoons is considered as a Poisson process. A functional choice for Poisson intensity is a gamma distribution because this distribution is conjugate to the Poisson likelihood (Epstein 1985). The posterior probability of regime shift at each point in time is obtained by formulating a hierarchical approach with three layers (i.e., data, parameter and hypothesis). Because probability can be thought of as the mathematical language of uncertainty, the Bayesian inference shows its advantage over the deterministic estimation of change-point location for quantifying uncertainty. Due to the relatively small sample size analyzed in this study (i.e., 10 autumns in each decade), tests without the necessity of assumptions about sampling distribution are appropriate. The non-parametric rank-based Wilcoxon-Mann-Whitney test (Wilcoxon 1945; Mann and Whitney 1947) is therefore used to assess the differences of mean fields for the two decades (Chu 2002).

## 3 Abrupt changes in autumn TC activity, large-scale circulation and ISO

Based on the RSMC-Tokyo, JTWC and STI best track data, there were ~11 TCs in each autumn over the WNP, accounting for 44% of the annual TC number (~25). Approximately 65% (7 out of 11) of these TCs were typhoons with destructive wind and heavy rain. Figure 1a shows the temporal variation of autumn typhoon count for the period 1977–2012. The time series of autumn typhoon count obtained from the JTWC, RSMC and STI are highly consistent (Fig. 1). The typhoon count dropped significantly since the late 1990s in all three best track datasets. An 11-year moving average is then applied to the time series derived from simple mean of the three datasets to extract the decadal variability in typhoon count. We can see that the typhoon count had positive (negative) anomalies before (after) 1997–1998 (Fig. 1a). To objectively detect the timing of abrupt decrease, we use the Bayesian change-point analysis, which estimates the posterior probability of each observation as a potential change point (Fig. 1b). The highest probability of a regime shift appeared in 1998 based on the RSMC and JTWC time series, suggesting that a new regime was likely to occur with 1998 being the first year. In the STI dataset, this year (1998) also showed a high probability of change-point occurrence, but its probability was slightly smaller than that in 1997. Since the three data averaged probability in 1998 was higher than that in 1997, we defined 1998 as the year when an abrupt change of typhoon count occurred. The decades before and after the occurrence of the regime shift are referred to as the active (1988–1997) and inactive (1998–2007) TC decades, respectively.

The differences in typhoon and TC counts in the active and inactive decades are listed in Table 1. The average typhoon count in each autumn dropped from 8 to 9 in the active decade to 6–7 in the inactive decade. This change is statistically significant based on the Mann–Kendall test. We further compare the TC counts over the WNP during the two decades. Similarly, all three best-track data reveal statistically significant increases in TC count during the active decade. On average, four more TCs were generated in each autumn during the active decade than during the inactive decade (Table 1). The average duration of TCs also tended to be longer during the active decade, although the change was of less significance. The ACE, which combines the information of TC count, intensity and lifespan, also appeared to be strengthened during the period of 1988–1997 (Table 1). Note that the differences in TC-related activity between the active and inactive decades are not sensitive to the definition of period length. The results using a 15-year period to define the active (1983–1997) and inactive (1998–2012) decades are consistent with the current results based on the 10-year period average (not shown).

Figure 2 displays the distributions of TC genesis (left panel) and frequency of occurrence (right panel) in the active and inactive TC decades. In autumn, the generation of TCs was concentrated in a zonally elongated area (7.5º–20ºN, 110º–170ºE) where the monsoon trough was located (Molinari and Vollaro 2013). During the active decade, increased TC geneses were observed east of the Philippine Sea (7.5º–20ºN, 130º–170ºE; Fig. 2a–c). The features of TC track could be approximately depicted by the TC frequency (Fig. 2d–f). During the active decade, more TCs developed westward toward the Philippine Sea and the South China Sea region (defined as the westward

Fig. 1 **a** Time series of autumn (SON) typhoon count in the WNP during 1977–2012. *Black, gray* and *hollow bars* illustrate the results from the RSMC-Tokyo, JTWC and STI datasets, respectively. The *dashed line* denotes the 11-year running mean of typhoon count based on the simple mean of the three datasets. **b** The posterior probability mass function of the change point as a function of time (year)
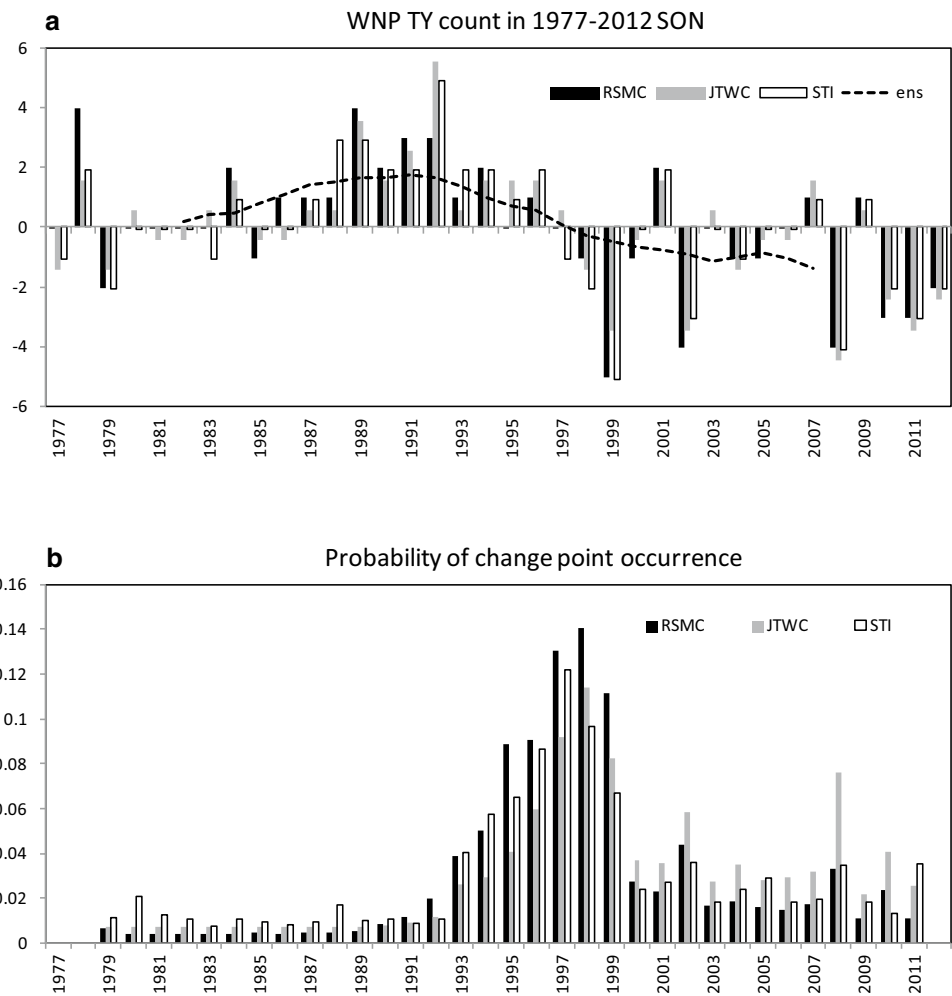
Table 1 Seasonal mean of typhoon count and TC count, lifespan (days) and ACE (10^3 m^{2}s^{-2}) of all TC cases for the active period (1988–1997) and inactive period (1998–2007), and the differences between the two epochs (active minus inactive period)

	JTWC			RSMC			STI		
	Active (88–97)	Inactive (98–07)	Diff	Active (88–97)	Inactive (98–07)	Diff	Active (88–97)	Inactive (98–07)	Diff
TY count	9.4	6.7	2.7*	8.7	6	2.7*	9.1	6.2	2.9*
TC count	13.3	9.7	3.6*	12.7	9.5	3.2*	12.7	9.1	3.6*
Lifespan (days)	6.23	5.13	1.1	5.83	5.09	0.74	5.97	3.99	1.98*
ACE(10^3 m^2 s^{-2})	39.7	32.1	7.6	30	24.8	5.2	28.7	23.32	5.38

*Indicate the decadal change is statistically significant at the 5% level based on the non-parametric Wilcoxon-Mann-Whitney rank-sum test. Results derived from the JTWC, RSMC_Tokyo and STI best track datasets are listed in the left, middle and right blocks, respectively

development region, WDR, of 7.5º–20ºN, 110º–130ºE) from the main genesis region (MGR, 7.5º–20ºN, 130º–170ºE). Meanwhile, TC frequency increased significantly to the east of Japan (30º–40ºN, 145º–165ºE), suggesting that the northeastward propagating and recurving TCs showed higher tendency to occur in the active TC decade (Fig. 2f). This region (30º–40ºN, 145º–165ºE) is referred to as the recurving to northeast (RNE). In contrast,

TC frequency of occurrence decreased over the East China Sea (ECS, 22.5º–35ºN, 120º–130ºE), which implies that TC landfall in Taiwan and southeast coast of China decreased, although the total TC number increased during the active TC decade.

Vigorous transient disturbances associated with SSEs and ISO may contribute to the enhanced TC activity during the active decade. As the seed disturbances, the WNP
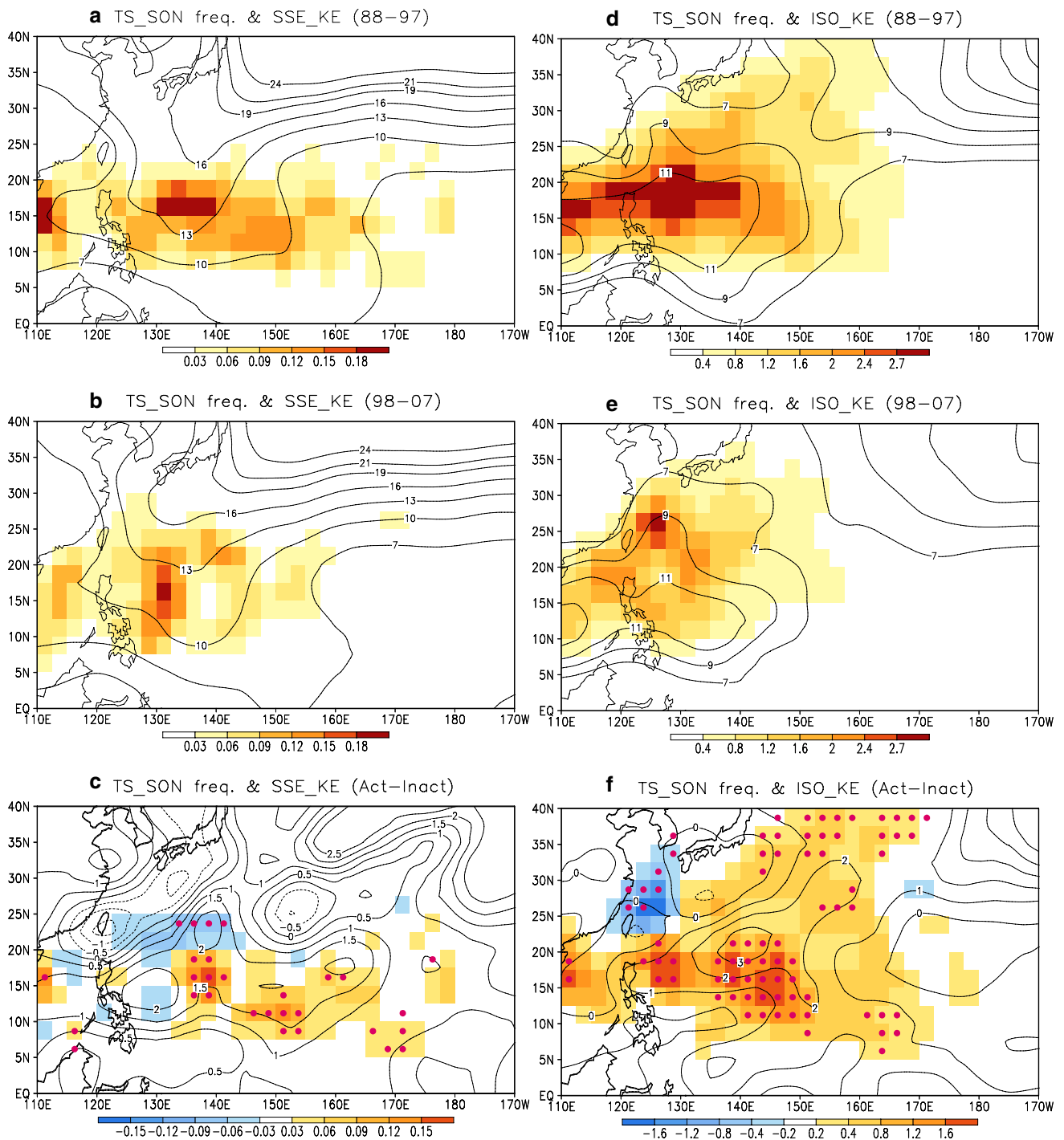
Fig. 2 The frequency of TC genesis derived from the JTWC (*shading*, number per season) and 850-hPa SSE KE (contour, m² s⁻²) during SON for (**a**) the period of 1988–1997 and (**b**) the period of 1998–2007, and (**c**) their difference (1988–1997 minus 1998–2007). **d–f** Same as (**a**)–(**c**), except that the shading indicates the frequency of TC occurrence and contours present the KE of 10–90-day ISO. The *red dots* in (**c**) and (**f**) mark the regions where the difference in TC genesis frequency between the two periods is statistically significant at the 5% level

SSEs were highly connected to the TC formation (Chang et al. 1996; Ritchie and Holland 1999). At the decadal timescale, the time series of SSE KE over the MGR reveals

a similar decadal variability to that of TC count. Enhanced SSE was observed more frequently before 1997, while weakened SSE tended to be dominant afterward. Based

on the Bayesian change-point analysis, the year with the highest probability of a regime shift was detected in 1998 (not shown), consistent with the change-point analysis result of TC count (Fig. 1b). This indicates that the growing (decreasing) SSE would provide more (less) precursor disturbances for TC genesis before (after) the late 1990s. In the composite of SSE KE during the active TC decade, the low-level SSE KE was strengthened and showed an eastward extension over the MGR (Fig. 2a). In contrast, during the inactive epoch the SSE KE tended to be reduced and confined within the subtropical western Pacific (Fig. 2b). The positive anomaly of SSE KE appeared coincidently over the area with increased TC genesis (Fig. 2c). This suggests a tight connection between the SSEs and WNP TC generation during autumn, consistent with the features found in summer (Maloney and Dickinson 2003; Hsu et al. 2011).

Figure 3 shows the structure and propagating feature of SSEs by plotting the lagged regression map of SSE vorticity field in the two decades. During both active (top row) and inactive (third row) decades, the 3–10-day vorticity was characterized by a northeast–southwest-oriented wave structure propagating northwestward over the tropical WNP, similar to the observed tropical depression-type (TD-type) disturbances in summer (Lau and Lau 1992; Takayabu and Nitta 1993). The synoptic wave trains were well organized and of higher amplitude during the active decade than during the inactive decade.

The strength of ISO also exhibited notable differences between the active TC decade and the inactive TC decade (Fig. 2d–f). The autumn ISO circulation revealed a zonally elongated structure moving northward from the equator toward the subtropical WNP (second and bottom rows in Fig. 3). Although the propagating features showed no significant changes between the two decades, the ISO vorticity tended to be amplified during the active TC decade (second row) compared to the inactive decade (bottom row). The KE of ISO was enhanced over most of the WNP with an exception over the vicinity of Taiwan and south of Japan (Fig. 2f). This anomalous ISO activity is mostly consistent with decadal changes in TC genesis count and frequency, suggesting the potential influence of ISO on TC formation and development.

Apart from the effects of transient disturbances on TC activity, the decadal change in seasonal-mean large-scale environment played a role in decreased TC activity in the recent decade (e.g., Liu and Chan 2013; He et al. 2015; Lin and Chan 2015; Hong et al. 2016). Figure 4 displays the differences in large-scale dynamic and thermodynamic factors that could influence TC activity during different decades. Compared to the SST in the inactive decade, significant cooling (warming) anomalies appeared in the WNP (the eastern equatorial Pacific) during the active decade,

which resembled an El Niño condition (Fig. 4a). This suggests that regional cooling over the WNP did not contribute to the vigorous TC activity over the WNP during the active TC decade (Liu and Chan 2013; Lin and Chan 2015). The lower tropospheric humidity (Fig. 4b) and vertical wind shear (Fig. 4e) both had slight changes over the MGR. In contrast, the dynamic effects associated with low-level vorticity (Fig. 4d) and vertical velocity in the mid troposphere (Fig. 4f) induced convective heating anomaly (Fig. 4c) over the MGR, creating a favorable condition for the generation of TCs during the active decade. Previous studies (e.g., Chan 2008) highlighted the importance of dynamic effects on TC activity over the WNP.

Based on Figs. 2 and 4, we observe that the autumn-mean cyclonic circulation, ISO activity and SSEs were all enhanced over the tropical WNP (including the MGR and WDR) and the mid-latitude region to the east of Japan (RNE) during the active TC decade. The extent of scale interactions among SSEs, ISO and seasonal-mean flow associated with the decadal change of TC activity and how the interactions worked will be examined quantitatively from the viewpoint of eddy energetics in the following section.

4 Diagnosis of SSE KE conversion processes

4.1 Eddy energetics over the main genesis region

To understand the physical processes responsible for the decadal change in SSE KE associated with TC genesis, the SSE KE budget equation was diagnosed. The enhanced (reduced) SSE KE was attributed to the accumulation (dissipation) of SSE KE related to a positive (negative) SSE KE tendency ($\overline{\partial K'/\partial t}$) during the active (inactive) decade. The decadal variability in SSE KE tendency over the MGR was highly connected with TC genesis count (Fig. 5) with high correlation coefficients (above ~0.9 for both TS and typhoon cases). The enhanced SSE KE tendency would favor the enhancement of precursor SSE disturbances for TC genesis during the active decade. The percentage of TDs developing into TCs during the active decade was around 93.5%, while it reduced to about 86.5% during the inactive decade, based on the JTWC and STI data (not shown). This suggests the significant influence of SSE activity on WNP TC genesis count.

The budget terms of CK, CE and BG were all positive over the MGR and tended to have higher amplitude during the active decade than during the inactive decade, contributing positively to the increased growth rate of SSE KE. The advection term (AK), however, decreased slightly during the active decade over the MGR (not shown). Because CK and CE were the real sources or
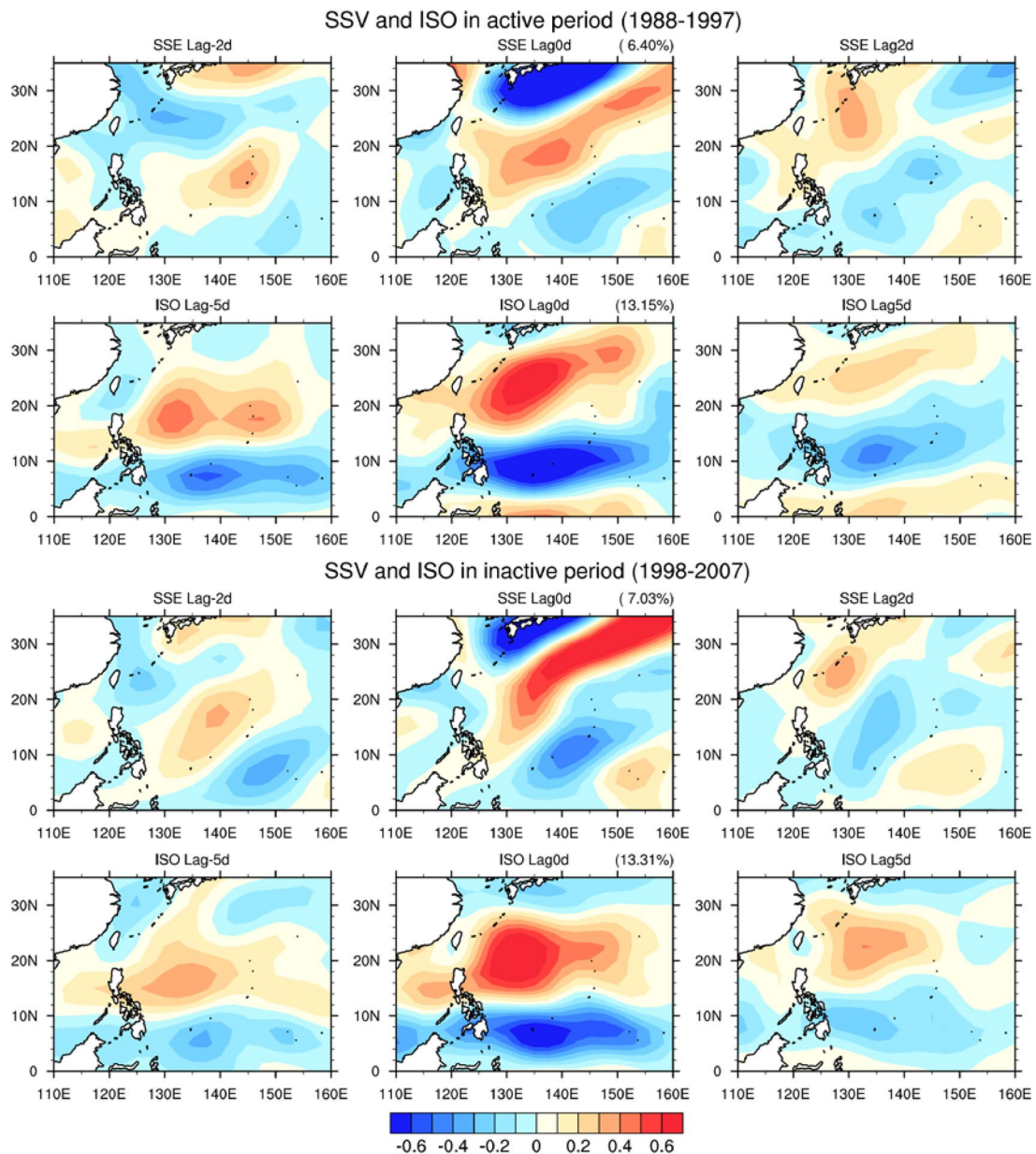
Fig. 3 Top row: 850-hPa synoptic-scale (3–10 days) vorticity (shading; 10^{-5} s^{-1}) regressed onto the principle component of the first EOF of 3–10-day vorticity over the western Pacific (100°–160°E, 0°–35°N) from day −2 to day +2 during SON of 1988–1997. Second row: Same as the top row, except for the lag–regression map of 10–90-day vorticity at 850 hPa. The two lower rows are the same as the two upper rows, except for the inactive period (1998–2007). The contributions of EOF1 to the total variance for each case are listed above each panel in the middle column

sinks of SSE KE, and other processes (BG and AK) were related to the redistribution of SSE KE, in the following we focus on how CK and CE modulated SSE KE and its tendency at the decadal timescale. Consistent with previous studies of climatological eddy energetics (Lau and Lau 1992; Maloney and Dickinson 2003), the positive CK maximized in the lower troposphere (Fig. 6a, b), where the SSE KE was the largest. This indicates that the major source of SSE KE over the tropical WNP was the low-level background flows. During the active decade, the low-level CK increased significantly over the MGR and WDR (Figs. 6c, 7a). In contrast to CK, CE played a role in providing KE to SSEs in the upper troposphere (Fig. 6d–f). The positive correlation between SSE temperature and vertical motion in the upper troposphere was enhanced over the tropical WNP during the active decade (Figs. 6f, 7b), suggesting that the SSEs obtained more KE from the conversion of SSE available potential
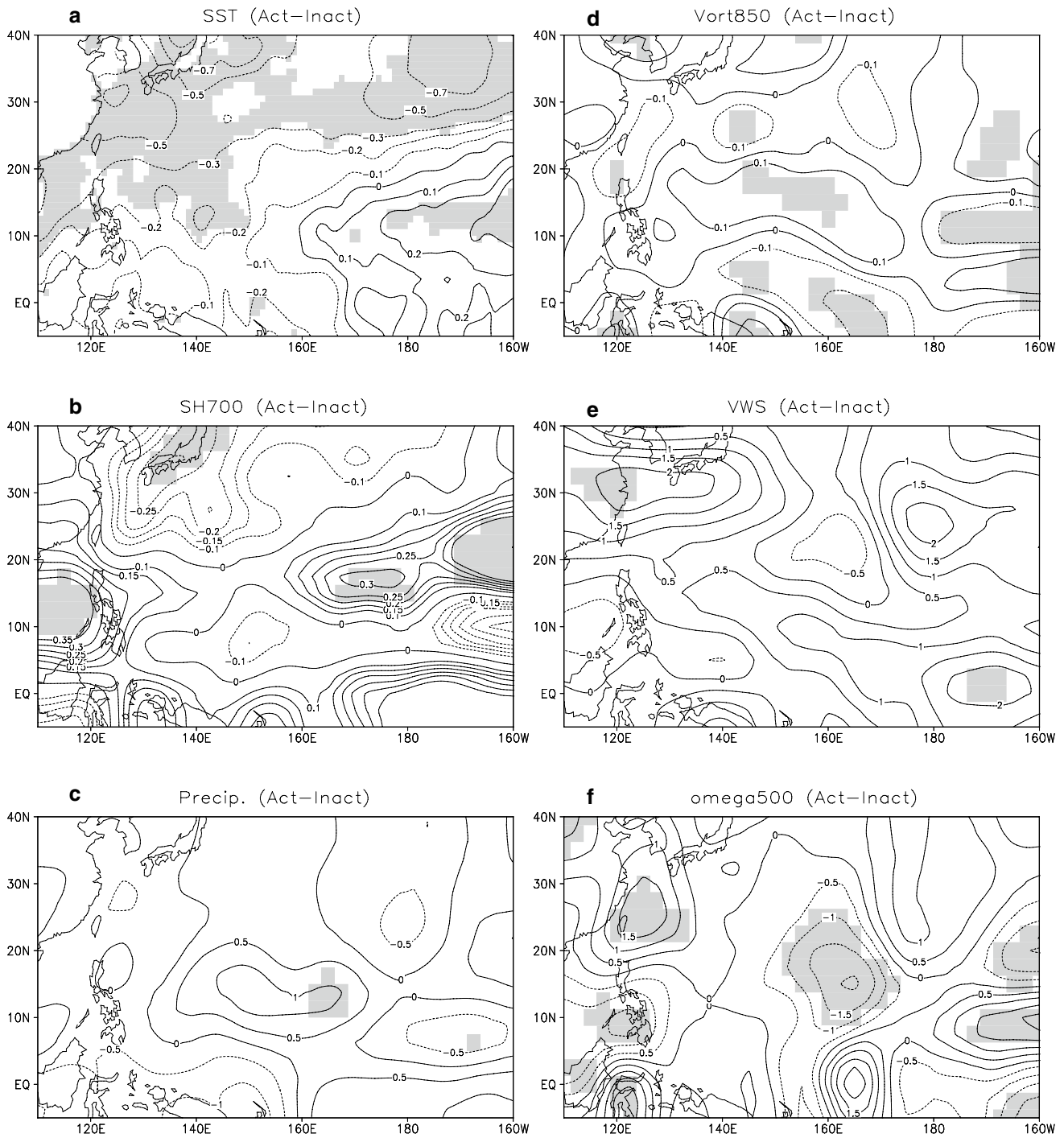
Fig. 4 Decadal changes in the large-scale environment during SON (1988–1997 minus 1998–2007) for (**a**) SST (K), (**b**) 700-hPa specific humidity (10^{-3} kg kg$^{-1}$), (**c**) precipitation (mm day^{-1}), (**d**) 850-hPa vorticity (10^{-5} s^{-1}), (**e**) vertical wind shear (m s^{-1}), and (**f**) p-velocity at 500 hPa (10^{-2} pa s^{-1}). *Shading marks* the region where the difference between the two periods is statistically significant at the 5% level

energy during the active TC decade than during the inactive decade.

CK includes the barotropic energy conversions related to mean flow–SSE interaction (CK_{M-S}) and ISO–SSE interaction (CK_{I-S}). CK_{M-S} (Fig. 7c) and CK_{I-S} (Fig. 7d) showed

comparable contributions to the enhanced SSEs in the tropical WNP (MGR and WDR) during the active TC decade. Thus, both the autumn mean flow and ISO provided more KE to the SSEs (including TCs) during the active decade than during the inactive decade. To explore the key

Fig. 5 Anomalies of autumn (SON) SSE KE tendency (*left axis*, units: 10^{-6} m^{2}s^{-3}) and TC count (*right axis*) in the WNP during 1977–2012 derived from (**a**) JTWC, (**b**) RSMC_Tokyo and (**c**) STI datasets. *Blue, green and red curves* represent the numbers of TD, TS and typhoon, respectively. An 11-year running mean is applied to all the time series to focus on their decadal variations. Correlation coefficients between the SSE KE tendency and TC count are listed at the *upper right corner* in each *panel*
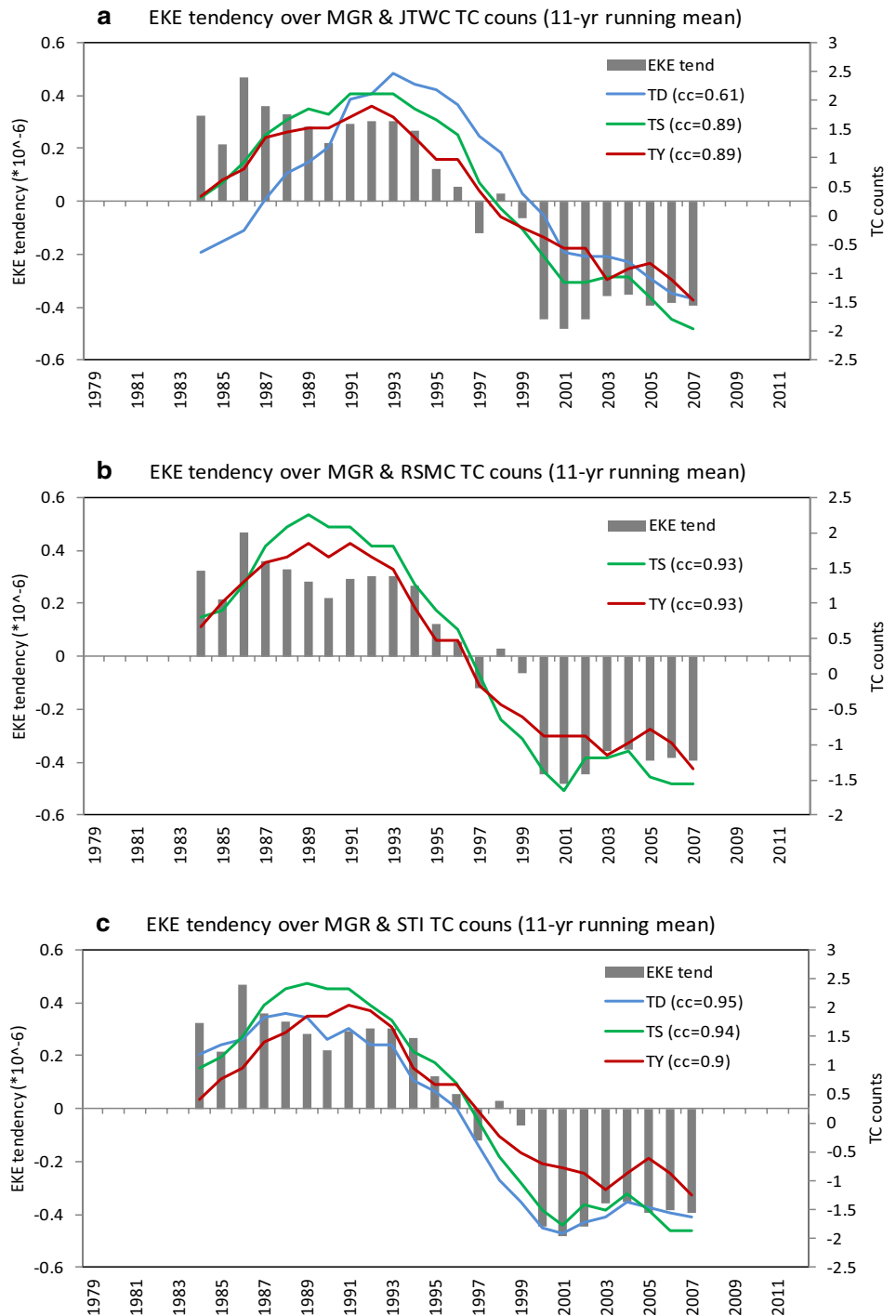
processes that determined the enhanced barotropic energy conversion for the growth of SSE KE and then the TC genesis, the decadal changes in each term of CK$_{M-S}$ and CK$_{I-S}$ were examined over the MGR (Fig. 8). The leading process of enhanced CK$_{M-S}$ was associated with the horizontal eddy momentum flux interacting with a meridional gradient of mean zonal wind ($-\overline{u'_s v'_s} \partial \tilde{u}/\partial y$). The synoptic eddies were characterized by a northeast–southwest-tilted wave train over the tropical WNP (Fig. 3). A positive horizontal momentum transport ($\overline{u'_s v'_s}$) of SSEs was always present in the MGR during the two decades (Fig. 9a, b). The sign of $-\overline{u'_s v'_s} \partial \tilde{u}/\partial y$ was thus determined by the meridional gradient of zonal mean flow. Over the MGR where the monsoon trough ($-\partial \tilde{u}/\partial y > 0$) was located, the SSEs could persistently gain KE from the cyclonic mean flow through a positive barotropic energy conversion ($-\overline{u'_s v'_s} \partial \tilde{u}/\partial y > 0$). As the
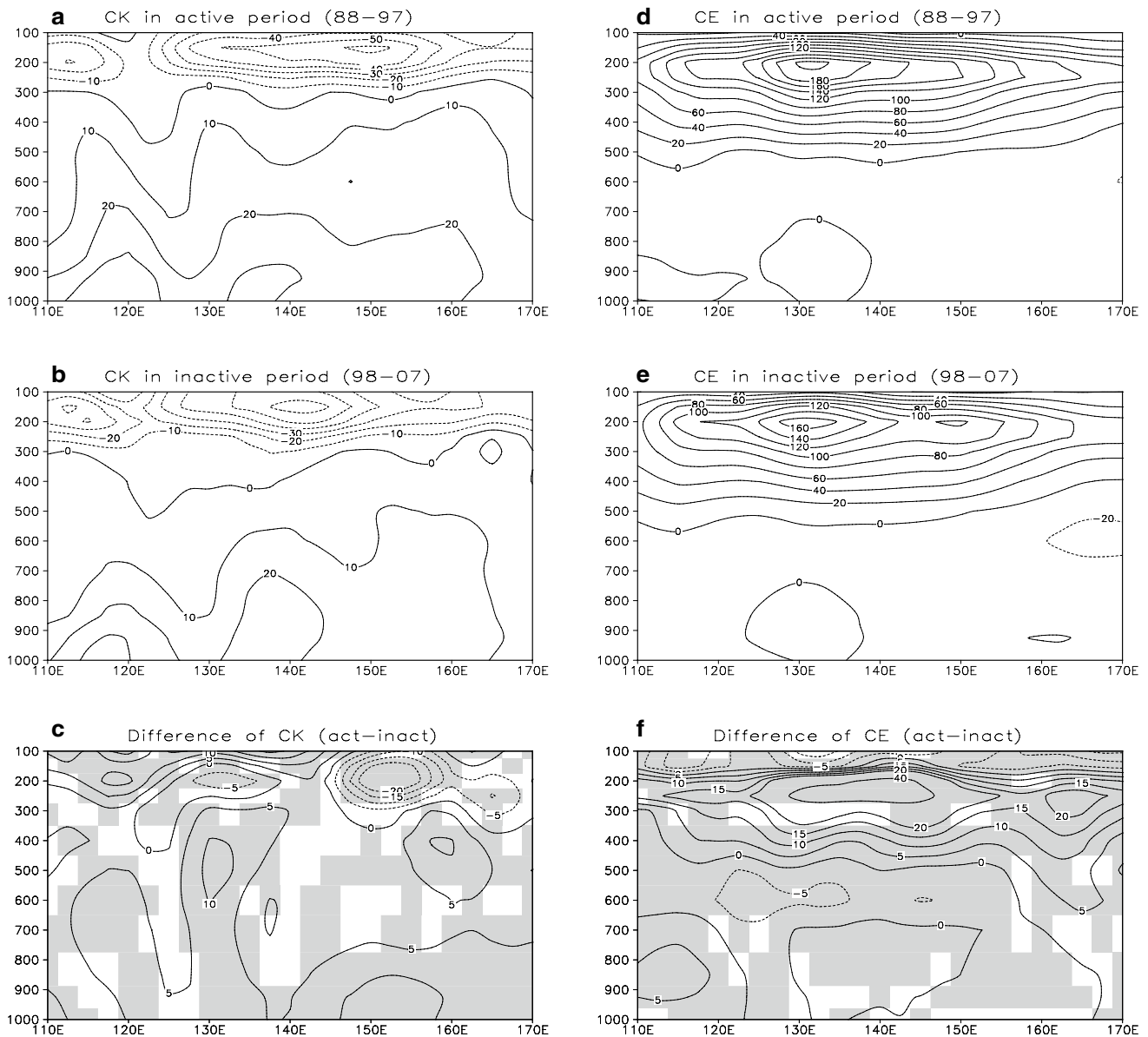
Fig. 6 *Vertical cross sections* of eddy barotropic energy conversion (10^{-6} m^{2}s^{-3}) along 10°–20°N with high TC genesis frequency in autumn for (**a**) the active period (1988–1997) and (**b**) the inactive period (1998–2007), and (**c**) the difference between the two periods (active minus inactive period). Shading in (**c**) marks the region where the difference between the two periods is statistically significant at the 5% level. **c**–**f** are the same as (**a**)–(**c**), except for the eddy baroclinic energy conversion

monsoon trough was strengthened during the active decade (Fig. 9c), enhanced cyclonic shear contributed positively to the growth of SSE KE over the MGR. The importance of the monsoon trough to TC genesis was documented in numerous studies (e.g., Holland 1995; Molinari and Vollaro 2013). Here, we further point out that the interaction between monsoon cyclonic shear and SSE momentum flux was the key process leading to the changes in SSE activity and associated TC genesis at the decadal timescale. Note that the zonal eddy momentum transport interacting with zonal mean flow convergence ($-\overline{u'_s u'_s} \partial \tilde{u}/\partial x$) was important

to the growth of SSEs during both active and inactive TC decades (Sobel and Bretherton 1999; Kuo et al. 2001). However, it was not responsible for the decadal change of TC genesis over the tropical WNP (Fig. 8a).

Along with the CK$_{M-S}$ process, the scale interaction between ISO and SSEs (CK$_{I-S}$) was another contributor to the vigorous SSEs over the MGR during the active decade (Fig. 7d). Figure 8b shows the leading terms of CK$_{I-S}$ during the active and inactive decades. Among these CK$_{I-S}$ processes, the term $-\overline{u'_s v'_s} \partial u'_I/\partial y$ showed the most significant impact on the decadal change in SSE KE over
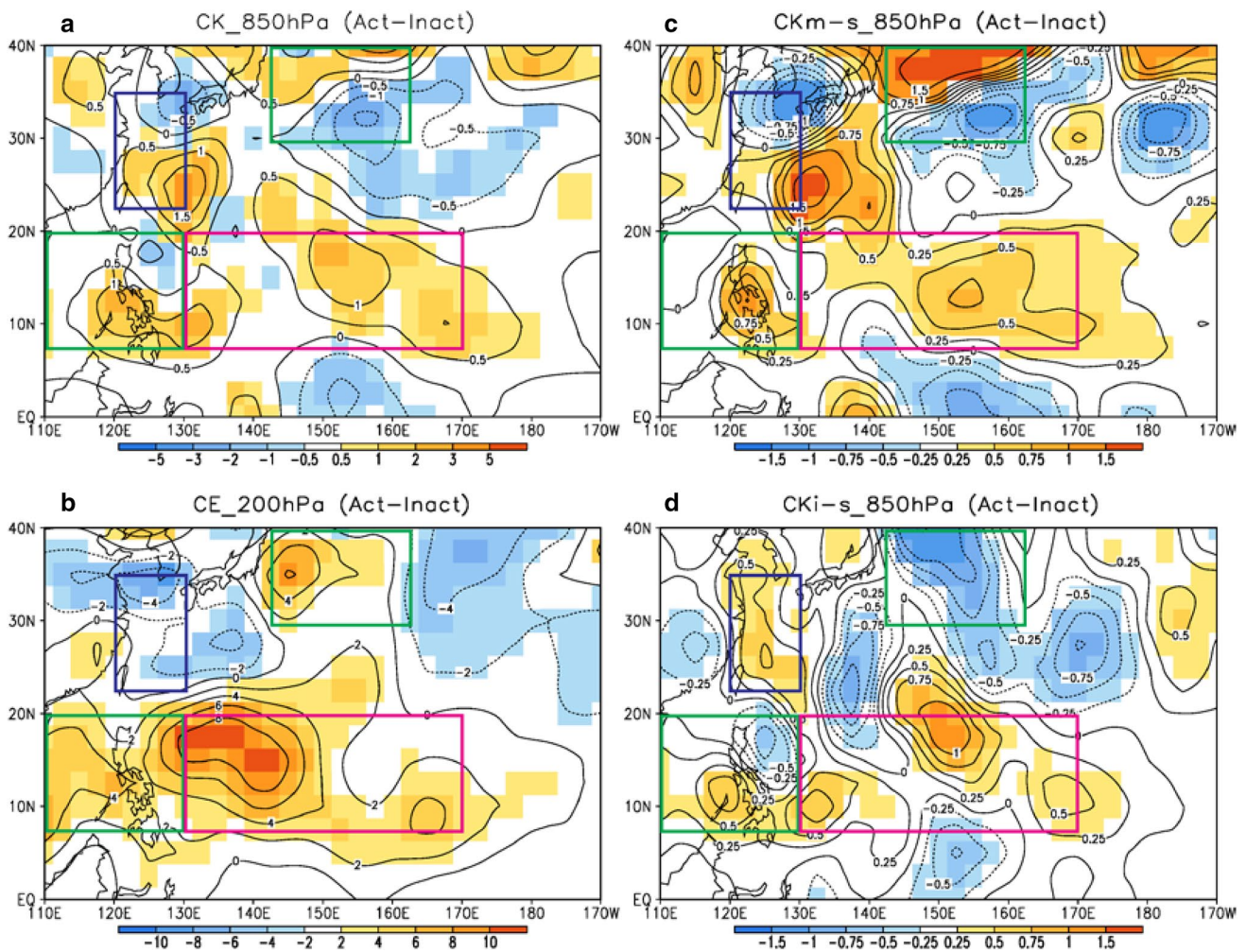
Fig. 7 Differences in (**a**) eddy barotropic energy conversion at 850 hPa and (**b**) eddy baroclinic energy conversion at 200 hPa between active and inactive periods. Units: 10^{-5} m^2 s^{-3}. Shading marks the region where the difference is statistically significant at the 5% level. *Red box* represents the MGR; *green boxes* indicate the the MGR. As discussed earlier, the northeast–southwest-oriented SSE wave train always induced a positive eddy momentum flux ($u'_s v'_s > 0$). This eddy momentum flux, however, was modulated by ISO phases (Maloney and Dickinson 2003). During the cyclonic phase ($-\partial u'_I/\partial y > 0$) of the ISO, the WNP eddy momentum flux tended to be enhanced in both active and inactive decades (Fig. 10c, d). Thus, the SSEs might continually gain KE from the ISO during the cyclonic phase of the ISO. In contrast, $u'_s v'_s$ became weakened during the anticyclonic ($-\partial u'_I/\partial y < 0$) phase of the ISO (Fig. 10e, f). The reduced amplitude of eddy momentum flux might attribute to the upscale KE conversion from the SSEs to ISO occured during the anti-cyclonic phase of the ISO (Hsu et al. 2011; Tsou et al. 2014). Because the sign and amplitude of $-u'_s v'_s \partial u'_I/\partial y$ depend on the cyclonic/anticyclonic phases of the ISO,

WDR and RNE with increased TC frequency in the recent decade; and *blue box* shows the ECS with decreased TC frequency in the recent decade. **c** and **d** are the same as (**a**), except for the barotropic energy conversion from mean flow and ISO to SSE, respectively
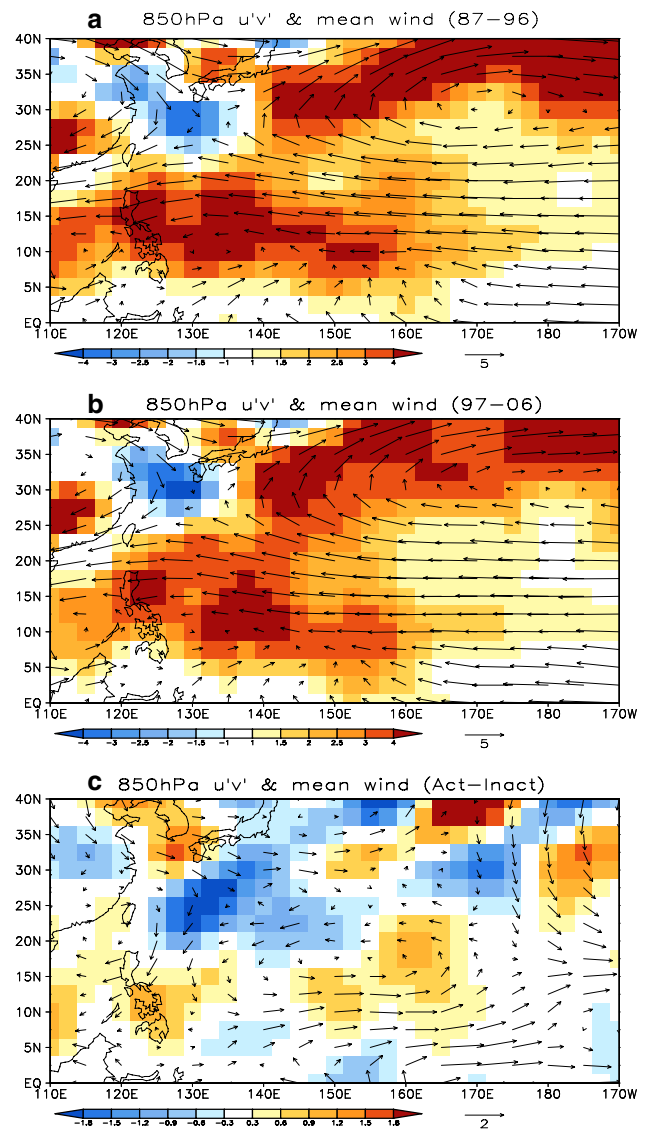
the frequency and amplitude of cyclonic/anticyclonic flow of the ISO in each decade largely accounted for the decadal change of $-u'_s v'_s \partial u'_I/\partial y$. Figure 9a reveals the probability density functions of ISO vorticity during the active and inactive decades. It is clear to see that the frequency and amplitude of ISO cyclonic (positive vorticity) flows were both increased considerably during the active TC decade compared to those in the inactive decade. The enhanced cyclonic circulation of the ISO led to the enhancement of $-u'_s v'_s \partial u'_I/\partial y$ during the active decade, even though the eddy momentum transport ($u'_s v'_s$) revealed a similar effect associated with various ISO phases in both decades (Fig. 10c–f). In summary, the increase and enhancement of active (cyclonic) phase of the ISO would favor the SSE growth and TC genesis through ISO–SSE interaction during the active TC decade.
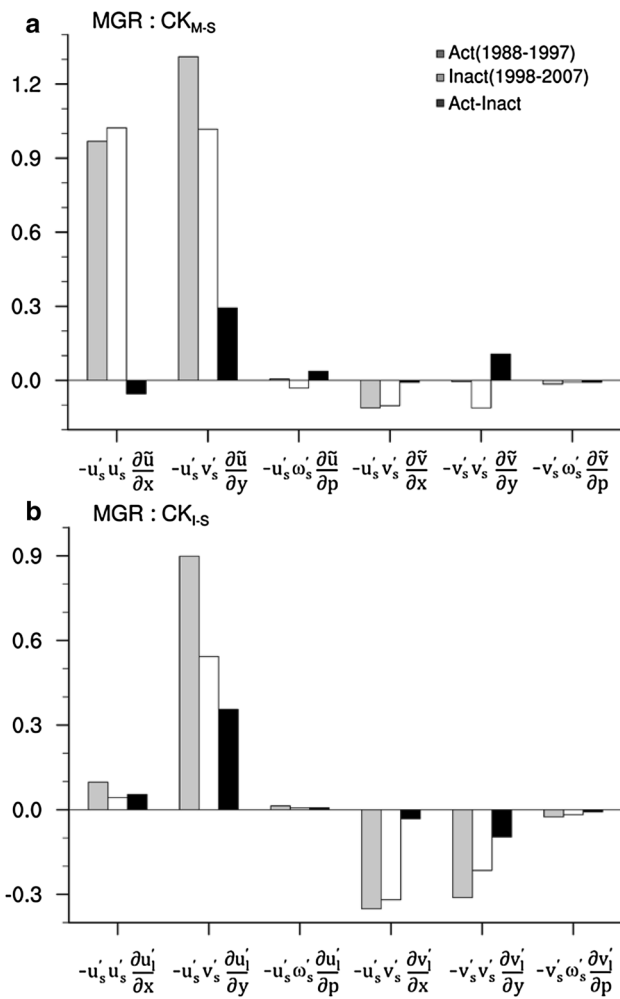
Fig. 8 (a) Each term of CK_{M-S} in autumn during the active period (*gray*) and inactive period (*white*), and their difference (*black*) averaged over the MGR (130°–170°E, 7.5°–20°N) with increased TC genesis during the active decade. (b) Same as (a), except for CK_{I-S}. Units: 10^{-6} m^2 s^{-3}

Fig. 9 Distributions of eddy momentum flux ($u'v'$) (*shading*, units: m s^{-1}) and seasonal-mean wind field (vector, units: m s^{-1}) in autumn during (**a**) the active period (1988–1997) and (**b**) inactive period (1998–2007), and (**c**) the difference between the two periods (active minus inactive period)

## 4.2 Eddy energetics associated with TC development/movement

During the active TC decade, TCs tended to develop westward and northeastward into the WDR and RNE after being generated over the MGR (Fig. 2f). Meanwhile, the number of TCs moving toward the ECS decreased. The energy sources of SSEs associated with TC development in different regions could be seen in Fig. 7 and Table 2. The increased SSE KE with westward propagating TCs was contributed by enhanced CK and CE. As the TC developed northward, the CE process became the dominant in supporting the SSE activity. The scale interaction process (CK), however, contributed negatively to the decadal change in TC frequency over the extratropical area. As shown in Table 2, the area-averaged CK over the RNE

(ECS), where the TC frequency increased (decreased), tended to be weakened (strengthened) during the active TC decade. The important role of CE process in subtropical eddy growth and TC intensification was documented in previous studies (Kung 1977; Lau and Lau 1992; Emanuel et al. 2004; Hsu et al. 2009).

To identify the key processes of mean flow–SSE and ISO–SSE interactions that contributed positively to the increased TC frequency over the Philippine Sea and the South China Sea, individual terms of CK_{M-S} and CK_{I-S} were averaged over the WDR and compared (Fig. 11). The leading term of positive CK_{M-S} anomaly was related to the
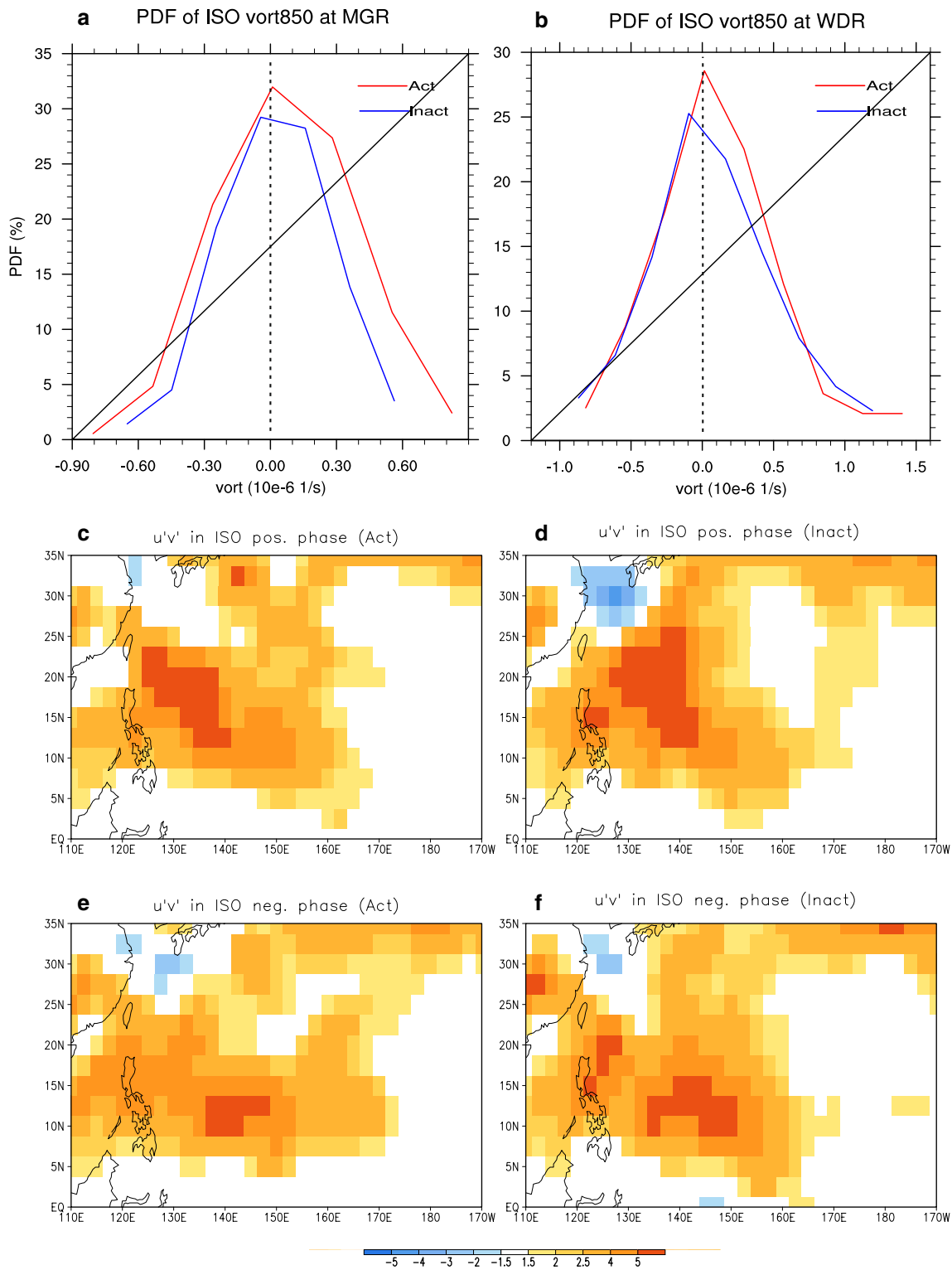
Fig. 10 **a** Probability density function of 850-hPa vorticity (units: $10^{-6}s^{-1}$) over the MGR in autumn during the active period (*red curves*) and inactive period (*blue curves*). **b** Same as (**a**), except for the WDR vorticity. **c, d** Composites of eddy momentum flux ($u'v'$, unit: $m^2 s^{-2}$) during the positive and negative vorticity periods of the ISO, respectively, during the active decade (1988−1997). **e, f** Same as **c, d**, except for the composites during the inactive decade (1998−2007)

Table 2 First and second rows: differences in low-level (850-hPa) and 1000–100-hPa averaged barotropic energy conversion averaged over the MGR (130°–170°E, 7.5°–20°N), WDR (110°–130°E, 7.5°–20°N), RNE (145°–165°E, 30°–40°N), and ECS (120°–130°E, 22.5°–35°N) between active and inactive decades

	MGR	WDR	RNE	ECS
CK850	0.74	0.53	−0.21	0.50
CK_zavg	0.33	0.49	−1.87	2.16
CE200	4.43	3.93	1.04	−2.42
CE_zavg	0.46	0.25	2.55	−0.36

Third and bottom rows: same as those in the two top rows, except for the high-level (200-hPa) and 1000–100-hPa averaged baroclinic energy conversion. Units: 10^{-5} m^{2}s^{-3}
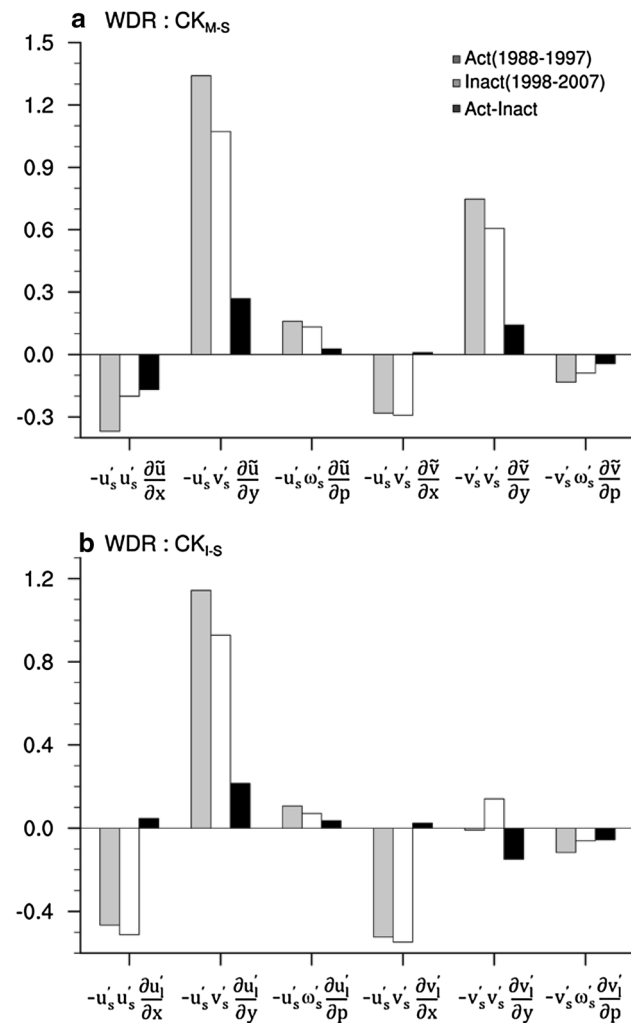
Fig. 11 Same as Fig. 8, except for the CK processes averaged over the WDR

mean cyclonic flow interacting with eddy momentum flux $(-\overline{u'_s v'_s} \partial \tilde{u}/\partial y)$. During the active TC decade, the strengthened monsoon trough induced a cyclonic anomaly over the

Philippine Sea and the South China Sea region (Fig. 9c), which resulted in enhanced KE conversion from seasonal-mean flow to SSEs. The increased SSE KE over the WDR maintained TC development when it moved westward after its generation. The secondary contributor was associated with the meridional component of mean flow convergence $(-\overline{v'_s v'_s} \partial \tilde{v}/\partial y)$. The enhancement of mean flow convergence created a favorable condition for the growth of SSEs/TCs over the South China Sea (Fig. 9c).

Consistent with the results of CK_{I-S} diagnosis related to TC genesis, the higher probability of occurrence of ISO cyclonic anomaly (Fig. 10b) contributed to the higher SSE KE converted from the ISO via the process of $-\overline{u'_s v'_s} \partial u'_I/\partial y$ over the WDR (Fig. 11b). The intensified ISO activity was related to the significantly increased low-level moisture content over the Philippine Sea and the South China Sea during the active TC decade (Fig. 4b). The low-level moistening was a critical factor for ISO development and strengthening (Wang and Xie 1997; Hsu and Li 2012).

5 Summary

The autumn (SON) TC activity over the WNP experienced a remarkable decadal change over the last three decades, similar to the variability in annual and peak-season TCs in this basin (e.g., Chan 2008; Liu and Chan 2013; Choi et al. 2015; He et al. 2015; Lin and Chan 2015). Based on the Bayesian change-point analysis, a change-point was detected in 1998. The decade before the occurrence of change point (1988–1997) had active TC-related features, such as increased TC genesis count, duration and intensity. TCs tended to move westward and recurved toward northeast, leading to a higher frequency of TC occurrence over the Philippine Sea, the South China Sea and east of Japan during the active TC decade. In contrast, the decade after 1998 (1998–2007) was characterized by an inactive TC period, although the sectors of Taiwan and southeast coast of China suffered from increased TC frequency in the recent decade (Hsu et al. 2014; Hong et al. 2016).

Negative SST anomaly appeared over the WNP during the active TC decade, suggesting that local ocean condition was not the key factor inducing the decadal change in TC activity (Liu and Chan 2013; Choi et al. 2015; He et al. 2015). Instead, during the active decade, the autumn-mean cyclonic anomaly, enhanced ISO and SSEs all appeared over the MGR with increased TC genesis count (7.5°–20°N, 130°–170°E). Meanwhile, enhanced KE of transient disturbances was observed in the regions with higher TC occurrence, including the WDR (7.5°–20°N, 110°–130°E) and RNE (30°–40°N, 145°–165°E). Using the SSE KE budget equation, which separates the effects of mean flow and ISO on SSEs, we examined how the internal

atmospheric processes associated with multi-scale interaction contributed to the decadal change in autumn SSEs and related TC activity. The major findings of this study are summarized in the schematic diagram (Fig. 12).

During the active TC decade, the seasonal-mean cyclonic anomaly associated with strengthened monsoon trough was observed in the tropical WNP. Through primarily the interaction between meridional gradient of zonal mean flow and eddy momentum flux $(-\overline{u'_s v'_s} \partial \tilde{u}/\partial y)$, the SSEs gained more KE from the mean flow ($CK_{M-S} > 0$). The increased probability of occurrence of intraseasonal cyclonic anomaly, during the active decade, also contributed positively to the SSE growth via the ISO–synoptic barotropic energy conversion ($CK_{I-S} > 0$). As the seed disturbances for TC formation, the enhanced SSEs could lead to higher TC genesis count over the MGR.

The atmospheric scale interaction over the tropics also played a role in supporting the succeeding development of TCs during the active TC decade. The cyclonic and convergent mean flow anomaly over the Philippine Sea and the South China Sea favored a positive CK_{M-S} anomaly when it interacted with eddy momentum flux. The enhanced ISO activity caused positive CK_{I-S} anomaly. Thus, the increased SSE KE obtained from both mean flow and ISO was favorable for the westward development of TCs toward the Philippine Sea and the South China Sea. In addition to the scale interaction, TCs could maintain themselves through the SSE baroclinic energy conversion. An increased CE also provided increased KE to the growth of SSEs/TCs when it propagated westward.

Fig. 12 Schematic diagram summarizing the eddy energetic processes associated with the change in autumn TC activity over the WNP during the active TC decade

As the SSEs/TCs moved northward into the subtropical/mid-latitude regions, the source of their KE was dominated by the CE process rather than the CK process (Kung 1977; Lau and Lau 1992; Emanuel et al. 2004; Hsu et al. 2009). During the active TC decade, increased (decreased) CE appeared over the RNE (ECS) where the TC frequency of occurrence increased (decreased). During the active TC decade, the increased KE of SSEs over the WDR and RNE could support the growth of TCs with intensified strength and longer lifespan.

The abrupt change in WNP TC and the related large-scale conditions were reported in a number of recent studies (Liu and Chan 2013; Choi et al. 2015; He et al. 2015; Hong et al. 2016; Lin and Chan 2015). However, the physical processes and quantitative contributions of mean flow–ISO–SSE interaction to TC-related SSEs activity were not well documented or explicitly shown. Based on the SSE energetic diagnosis, we found that both mean flow and ISO variations at the decadal timescale played important roles in causing the abrupt decrease in TC activity during the recent decade. The mechanisms inducing the cyclonic mean flow and enhanced ISO anomalies during the active decade need to be investigated. Previous studies found different SST modes over the globe can modulate WNP TC activities through altering the large-scale circulation associated with TC genesis and development. For example, the cyclonic shear associated with monsoon trough extends southeastward during the El Niño years (Chan 2000; Wang and Chan 2002), resulting in increased TC genesis near the dateline. Based on a series of model experiments, Hsu et al. (2014) and Zhang et al. (2016a) suggested that the cyclonic anomalies conducive to TC genesis over the WNP might be induced by the warm SST anomalies over the tropical and extratropical central-eastern Pacific as a Rossby wave response, resembling a classic Gill pattern (Gill 1980). In addition to the Pacific basin, the SST anomalies over the Indian Ocean play a role in modulating the WNP TC activityh (Du et al. 2010; Zhan et al. 2010). The warming (cooling) in the Indian Ocean may force a warm (cold) tropospheric Kelvin wave propagating eastward into the western Pacific and then induce anticyclonic (cyclonic) anomaly over the WNP TC genesis region. Recently, Huo et al. (2015), Yu et al. (2016) and Zhang et al. (2016b) highlighted the remote effects of Atlantic SST on the WNP TC activity via influencing the large-scale circulations over the WNP.

The major findings based on the observational data in this study also imply that correct simulation of not only mean flow changes but also ISO variability is critical to improving the predictability of seasonal-mean TC count, duration and intensity at a long-term (decadal) timescale. Currently, some general circulation models display high fidelity of ISO periodicity and propagation, but some show
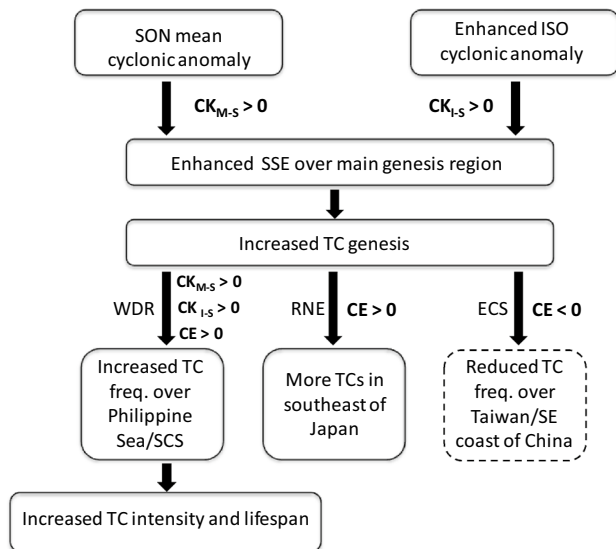
limited skill in capturing the ISO-related features (e.g., Klingaman et al. 2015). In the future, we will assess model capability in multi-scale interaction and try to understand the sources of simulation biases.

References

Bell GD et al (2000) Climate assessment for 1999. Bull Amer Meteor Soc 81:S1–S50

Chan JCL (2000) Tropical cyclone activity over the western North Pacific associated with El Niño and La Niña events. J Clim 13:2960–2972

Chan JCL (2008) Decadal variations of intense typhoon occurrence in the western North Pacific. Proc R Soc A 464:249–272

Chang C-P, Chen JM, Harr PA, Carr LE (1996) Northwestward-propagating wave patterns over the tropical western North Pacific during summer. Mon Wea Rev 124:2245–2266

Chen GH (2012) A comparison of the transition of equatorial waves between two types of ENSO events in a multilevel model. J Atmos Sci 69:2364–2378

Chen GH, Huang RH (2009) Interannual variation of the mixed Rossby-Gravity waves and their impact on tropical cyclogenesis in the western North Pacific. J Clim 22:535–549

Choi Y, Ha K-J, Ho C-H, Chung CE (2015) Interdecadal change in typhoon genesis condition over the western North Pacific. Clim Dyn 45:3243–3255

Chu P-S, 2002: Large-scale circulation features associated with decadal variations of tropical cyclone activity over the central North Pacific. J Climate, 15, 2678–2689

Chu P-S, Zhao X (2004) Bayesian change-point analysis of tropical cyclone activity: the central North Pacific case. J Clim 17:4893–4901

CMA (2014) Shanghai Typhoon Institute of China Meteorological Administration best track data. Available online at http://tcdata.typhoon.gov.cn/en/

Daubechies I (1988) Orthonormal bases of compactly supported wavelets. Commun Pure ApplMath 41:909–996

Du Y, Yang L, Xie S-P (2010) Tropical Indian Ocean influence on northwest Pacific tropical cyclones in summer following strong El Niño. J Clim 24:315–322

Emanuel KA (2005) Increasing destructiveness of tropical cyclones over the past 30 years. Nature 436:686–688

Emanuel KA, DesAutels C, Holloway C, Korty R (2004) Environmental control of tropical cyclone intensity. J Atmos Sci 61:843–858

Epstein ES (1985) Statistical inference and prediction in climatology: A Bayesian approach. Amer Meteor Soc 42:199

Gill AE (1980) Some simple solutions for heat-induced tropical circulation. Quart J Roy Meteor Soc 106:447–462

He H, Yang J, Gong D-Y, Mao R, Wang Y, Gao MN (2015) Decadal changes in tropical cyclone activity over the western North Pacific in the late 1990s. Clim Dyn 45:3317–3329

Holland GJ (1995) Scale interaction in the western Pacific monsoon. Meteor Atmos Phys 56:52–79

Hong C-C, Wu Y-K, Li T (2016) Influence of climate regime shift on the interdecadal change in tropical cyclone activity over the Pacific Basin during the middle to late 1990s. Clim Dyn. doi:10.1007/s00382-016-2986-x.

Hsu P-C, Li T (2012) Role of the boundary layer moisture asymmetry in causing the eastward propagation of the Madden-Julian Oscillation. J Climate 25:4914–4931

Hsu P-C, Yang Y (2015) Contribution of atmospheric internal processes to interannual variability of South Asian summer monsoon. Int J Climatol. doi:10.1002/joc.4528

Hsu P-C, Tsou C-H, Hsu H-H, Chen J-H (2009) Eddy energy along the tropical storm track in association with ENSO. J Meteor Soc Japan 87:687–704

Hsu P-C, Li T, Tsou C-H (2011) Interactions between boreal summer Intraseasonal oscillations and synoptic-scale disturbances over the western North Pacific. Part I: energetics diagnosis. J Clim 24:927–941

Hsu P-C, Chu P-S, Murakami H, Zhao X (2014) An abrupt decrease in the late-season typhoon activity over the western North Pacific. J Clim 27:4296–4312

Huo L, Guo P, Hameed SN, Jin D (2015) The role of tropical Atlantic SST anomalies in modulating western North Pacific tropical cyclone genesis. Geophys Res Lett 42:2378–2484

JTWC (2014) The Joint Typhoon Warning Center Western North Pacific best track data. Available online at http://www.usno.navy.mil/NOOC/nmfc-ph/RSS/jtwc/best_tracks/wpindex.html

Kamahori H, Yamazaki N, Mannoji N, Takahashi K (2006) Variability in intense tropical cyclone days in the western North Pacific. SOLA 2:104–107

Kanamitsu M, Ebisuzaki W, Woollen J, Yang S-K, Hnilo JJ, Fiorino M, Potter GL (2002) NCEP-DOE AMIP-II reanalysis (R-2). Bull Amer Meteor Soc 83:1631–1643

Klingaman NP, Jiang X, Xavier PK, Petch J, Waliser D, Woolnough SJ (2015) Vertical structure and physical processes of the Madden-Julian oscillation: synthesis and summary. JGR–Atmos 120:4671–4689

Klotzbach PJ, Landsea CW (2015) Extremely intense hurricanes: Revisiting Webster et al. (2005) after 10 years. J Clim 28:7621–7629

Knapp KR, Kruk MC, Levinson DH, Diamond HJ, Neumann CJ (2010) The international best track archive for climate stewardship (IBTrACS): Unifying tropical cyclone data. Bull Amer Meteor Soc 91:363–376

Ko K-C, Hsu H-H (2009) ISO modulation on the submonthly wave pattern and the recurving tropical cyclones in the tropical western North Pacific. J Climate 22:582–599

Kossin JP, Knapp KR, Vimont DJ, Murnane RJ, Harper BA (2007) A globally consistent reanalysis of hurricane variability and trends. Geophys Res Lett 34:L04815

Kossin JP, Olander TL, Knapp KR (2013) Trend analysis with a new global record of tropical cyclone intensity. J Clim 26:9960–9976

Kung EC (1977) Energy sources in middle-latitude synoptic-scale disturbances. J Atmos Sci 34:1352–1365

Kuo HC, Chen JH, Williams RT, Chang CP (2001) Rossby waves in zonally opposing mean flow: behavior in Northwest Pacific summer monsoon. J Atmos Sci 58:1035–1050

Lau K-H, Lau N-C (1992) The energetics and propagation dynamics of tropical summertime synoptic-scale disturbances. Mon Wea Rev 120:2523–2539

Lin I-I, Chan JCL (2015) Recent decrease in typhoon destructive potential and global warming implications. Nature Commun 6:7182

Liu KS, Chan JCL (2013) Inactive period of western North Pacific tropical cyclone activity in 1998–2011. J Clim 26:2614–2630

Maloney ED, Dickinson MJ (2003) The intraseasonal oscillation and the energetics of summertime tropical western North Pacific synoptic-scale disturbances. J Atmos Sci 60:2153–2168

Maloney ED, Hartmann DL (2001) The Madden–Julian oscillation, barotropic dynamics, and North Pacific tropical cyclone formation. Part I: observations. J Atmos Sci 58:2545–2558

Mann HB, Whitney DR (1947) On a test of whether one of two random variables is stochastically larger than the other. Ann Math Stat 18:50–60

Maue RN (2011) Recent historically low global tropical cyclone activity. Geophys Res Lett 38:L14803

Molinari J, Vollaro D (2013) What percentage of western North Pacific tropical cyclones form within the monsoon trough? Mon Wea Rev 141:499–505

Rayner NA, Parker DE, Horton EB, Folland CK, Alexander LV, Rowell DP (2003) Global analysis of sea surface temperature, sea ice, and night marine air temperature since the late nineteenth century. J Geophys Res 108:4407

Ritchie EA, Holland GJ (1999) Large-scale patterns associated with tropical cyclogenesis in the western Pacific. Mon Wea Rev 127:2027–2043

RSMC (2013) Regional Specialized Meteorological Centers–Tokyo Typhoon Center tropical cyclone data. Available online at http://www.jma.go.jp/jma/jma-eng/jma-center/rsmc-hp-pub-eg/track-archives.html

Simiu E, Scanlon RH (1978) Wind effects on structures. Wiley Interscience, New York, NY, p 458

Sobel AH, Bretherton CS (1999) Development of synoptic-scale disturbances over the summertime tropical northwest Pacific. J Atmos Sci 56:3106–3127

Song JJ, Wang Y, Wu LG (2010) Trend discrepancies among three best track data sets of western North Pacific tropical cyclones. J Geophys Res 115:D12128

Suhas E, Neena JM, Goswami BN (2012) Interannual variability of Indian summer monsoon arising from interactions between seasonal mean and intraseasonal oscillations. J Atmos Sci 69:1761–1774

Takayabu YN, Nitta T (1993) 3–5 day period disturbances coupled with convection over the tropical Pacific Ocean. J Meteor Soc Jpn 71:221–246

Tsou C-H, Hsu H-H, Hsu P-C (2014) The role of multi-scale interaction in synoptic-scale eddy kinetic energy over the western North Pacific in autumn. J Clim 27:3750–3766

Wang B, Chan JCL (2002) How strong ENSO events affect tropical storm activity over the Western North Pacific. J Clim 15:1643–1658

Wang B, Xie X (1997) A model for the boreal summer intraseasonal oscillation. J Atmos Sci 54:72–86

Webster PJ, Holland GJ, Curry JA, Chang H-R (2005) Changes in tropical cyclone number, duration, and intensity in a warming environment. Science 309:1844–1846

Wilcoxon F (1945) Individual comparisons by ranking methods. Biom Bull 1:80–83

Wu MC, Yeung KH, Chang WL (2006) Trends in western North Pacific tropical cyclone intensity. EOS Trans Am Geophys Union 87:537–538

Yu J, Li T, Tan Z, Zhu Z (2016) Effects of tropical North Atlantic SST on tropical cyclone genesis in the western North Pacific. Clim Dyn 46:865–877

Zhan R, Wang Y, Lei X (2010) Contributions of ENSO and East Indian Ocean SSTA to the interannual variability of northwest Pacific tropical cyclone frequency. J Clim 24:509–521

Zhang W, Vecchi G, Murakami H, Villarini G, Jia L (2016a) The Pacific meridional mode and the occurrence of tropical cyclones in the Western North Pacific. J Clim 29:381–398

Zhang W, Vecchi GA, Villarini G, Murakami H, Rosati A, Yang X, Jia L, Zeng F (2016b) Modulation of Western North Pacific tropical cyclone activity by the Atlantic Meridional Mode. Clim Dyn. doi:10.1007/s00382-016-3099-2